Reac Kinet Mech Cat (2016) 118:655–668
DOI 10.1007/s11144-016-1017-6

Preparation of manganese-impregnated alumina-pillared bentonite, characterization and catalytic oxidation of CO

M. Dhahri[1,3] · M. A. Muñoz[2] · M. P. Yeste[2] · M. A. Cauqui[2] · N. Frini-Srasra[1,3]

Received: 18 November 2015 / Accepted: 11 March 2016 / Published online: 23 March 2016
© Akadémiai Kiadó, Budapest, Hungary 2016

Abstract Al-pillared clays from local available bentonite were synthesized via two methods by the application of conventional and ultrasonic treatments during the intercalation stage. The results of XRD and N_2 adsorption indicated an increase in the basal spacing, the specific BET surface area, and porosity subsequent to pillaring by both methods with a considerable shortening of the intercalation process for the ultrasonic method. Al-pillared bentonites were used as supports to prepare manganese oxide catalysts by the wet impregnation of 2 and 10 wt% of Mn. The presence of MnO_2 and Mn_2O_3 were detected by X-ray diffraction and confirmed by temperature-programmed reduction for the higher loading catalyst with 10 wt% of Mn. The catalytic activity of our catalysts was evaluated in the CO oxidation reaction. According to our results, the concentration of the Mn seems to be the factor that decisively affects the catalytic activity at the expense of the preparation method.

Keywords Bentonite · Pillared clays · Ultrasonic · Impregnation · CO oxidation

Introduction

Carbon monoxide (CO) is a very toxic gas for humans and animals, produced by the incomplete combustion of any carbon substance. CO is in fact a colorless, tasteless, hazardous and odorless gas and for this reason it is the most common type of

✉ M. Dhahri
mouldidhahri@gmail.com

[1] Laboratoire de Physico-Chimie des Matériaux Minéraux et leurs Applications, Centre National des Recherches en Sciences des Matériaux, Technopole Borj Cédria, Soliman, Tunisia

[2] Departamento de Ciencia de los Materiales e Ingeniería Metalúrgica y Química Inorgánica, Facultad de Ciencias, Universidad de Cádiz, 11510 Puerto Real, Cádiz, Spain

[3] Département de Chimie, Faculté des Sciences de Tunis, Université El Manar, 1060 Tunis, Tunisia

gaseous poisoning and every year several people die for accidental exposure to this gas. For this reason, there is an urgent need of devices able to detect and signal a CO alarm [1–7]. Huge amounts of this gas are emitted in the world, mainly from the living process, volcanic activity or bushfires. The condition of the environment and the human health are directly related to the anthropogenic emission. There are numerous and different sources of CO formation, e.g. transport, energy production, agriculture, chemical and steel industry [8, 9]. One of the most important solutions for its elimination is the catalytic oxidation. The catalytic oxidation of CO has been of considerable interest recently due to its relevance in many industrial applications such as gas purification in CO_2 lasers, CO gas sensors, air-purification devices for respiratory protection, and pollution control devices for reducing industrial and environmental emission [10–12].

In the recent few years, a lot of catalysts were used in this reaction. Pillared clay (PILC) possesses several interesting properties, such as high surface area, large interlayer spacing, high thermal stability, special surface acidity. Due to their properties, PILC are very suitable to be used as adsorbents, catalysts and catalyst supports [13–21].

In order to get a faster and more effective method to prepare PILCs, the ultrasound irradiation was used. In the past few years, several works have reported the benefits of ultrasound for the reduction of the pillarization time. Thus for example, Pérez et al. [22] concluded that ultrasounds considerably reduce the modification time for solids, in fact in just 10 min they get the same effect to those obtained with prolonged synthesis method (24 h). Olaya et al. [23] reported the synthesis of PILC with and without ultrasound. They found that using ultrasound has the advantage of decreasing the consumption of water between 90 and 95 % as well as the processing time. Similar benefits were obtained by Tamoul [24] for the synthesis of zirconium-pillared bentonite.

The use of both noble metals [25–27] and transition metal oxides [28–30] supported on clays for the CO oxidation reaction has been well documented. In general, noble metals are highly active for the oxidation of CO, whereas they are expensive due to rareness. In contrast, transition metal oxides are less costly, and their catalytic activities can be optimized by tailoring their crystal structures, morphologies and surface properties during their synthesis [31–33].

Manganese oxides have been considered as one of the most promising transition metal oxide catalysts for oxidation reactions owing to their strong oxygen storage/release ability and excellent redox properties. The polyvalent property of manganese shows its highest catalytic activity in the complete oxidation of air pollutants [31, 34, 35].

The aim of our present study was to prepare environmentally friendly and cheaper catalysts based on manganese oxides supported on Al-pillared bentonite, which is an important clay mineral source in Tunisia. The characterization of catalysts was performed by X-ray powder diffraction (XRD), N_2 adsorption at 77 K and H_2 temperature programmed reduction (H_2-TPR) techniques. The catalytic activities of the resulting solids were investigated in the oxidation of CO.

Experimental

Materials

Natural bentonite from the Haidoudi deposit in the region of Gabes in southern Tunisia was used as a starting material in this work. The chemical composition of the natural bentonite is: SiO_2 63.30, Al_2O_3 22.35, Fe_2O_3 7.38, Na_2O 1.34, MgO 1.50, CaO 2.26, and K_2O 1.3, expressed in the oxide from 100 g^{-1} of calcined sample. The specific surface area $S_{BET} = 72$ m^2/g, pore volume $V_p = 0.131$ cm^3/g, $d_{001} = 15.37$ Å and the cation exchange capacity (CEC) is 65.1 meq/100 g.

In order to prepare the pillared materials, crude bentonite was purified and transformed into its sodium form by treatment with 1 mol/L solution of sodium chloride (NaCl). The Na-saturated bentonite was washed with deionized water until excess chloride ions were removed (silver nitrate test), and dried at 80 °C. Fig. 1 shows the diffractograms of Na-clay (normal untreated, heated at 550 °C and glycolated. The basal distance d_{001} of the normal Na-clay was 12.75 Å. After treatment with ethylene glycol, the d_{002} of smectite appeared at 8.89 Å, which is attributable to an interstratified illite smectite [36]. In addition, according to the chemical analysis, the average elemental structural formula of the Na-bentonite (denoted H) purified clay is $[Si_{7.312}Al_{0.688}]IV$ $[Al_{3.014}Fe_{0.656}Mg_{0.357}]VI$ O_{20} $(OH)_4Na_{0.714}$ $Ca_{0.037}$ $K_{0.174}$. Their specific surface area and total pore volume are about 118 m^2/g and 0.150 cm^3/g and its cation exchange capacity (CEC) is equal to 78 meq/100 g.

Synthesis of pillared clay

The pillaring solution was prepared by slow adding of a 0.2 M NaOH solution into a 0.1 M Al $(NO_3)_3 \cdot 9H_2O$ solution until the OH/Al (mole ratio) was equal to 2.4. The

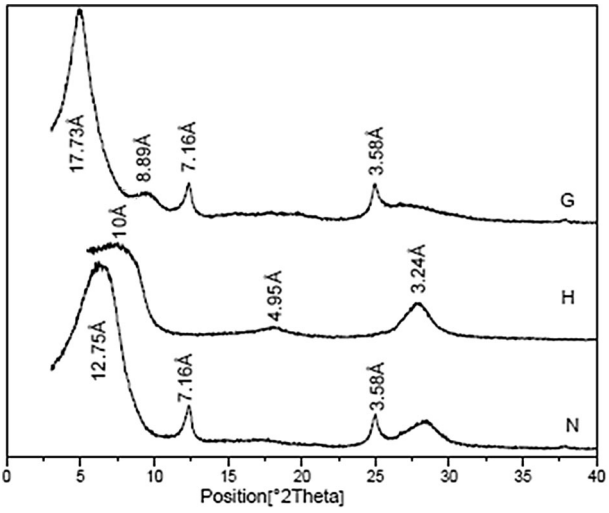

Fig. 1 X-ray diffraction patterns of the oriented Na-clay (fraction <2 μm) *N* normal untreated, *H* heated, *G* glycolated)

obtained mixture was aged at room temperature for 24 h under constant stirring. The pillaring solution was then added dropwise under stirring at room temperature to a bentonite suspension of 2 wt% prepared in deionized water and stirred for 2 h, maintaining a ratio of 10 mmol of total metal per gram of clay. The final clay suspension was later aged under two different conditions: (1) at room temperature for 24 h under constant stirring and (2) for 20 min in an ultrasonic bath (Bandelin Sonorex, operating frequency 35 kHz). The resulting product was separated by centrifugation and washed with distilled water by dialysis membranes (5 times) and dried at 80 °C, The sample was ground, sieved (106 meshes) and calcined at 500 °C for 2 h at a heating rate of 10 °C min^{-1}. The pillared bentonites prepared using the conventional treatment were labeled (Al–H) and the pillared bentonites prepared using the ultrasonic treatment were labeled (Al–H)*.

Catalyst preparation

The catalysts were prepared by the incipient wetness impregnation of the solids resulting from calcination at 500 °C for 2 h of the Al-PILC. The required volume of an aqueous solution of $Mn(NO_3)_2{\cdot}4H_2O$ was slowly added to the PILC to give solids with a content of about 2 and 10 wt% amount of manganese. The resulting material was subsequently dried at 80 °C and heated at 500 °C for 2 h. These catalysts were labeled as 2 % Mn (Al–H) or 2 % Mn (Al–H)* and 10 % Mn (Al–H) or 10 % Mn (Al–H)*.

Characterization

X-ray diffraction (XRD) patterns were recorded over powder solids using a PANalytical XPert-V diffractometer, with a scanning speed of 5°/min, employing Cu K_α filtered radiation ($\lambda = 1.5418$ Å).

The chemical analysis of the starting material and modified samples was performed on an Analytik Jena model Vario 6 flame atomic absorption spectrophotometer (FAAS).

Surface area (S_{BET}) values were obtained from the nitrogen adsorption/desorption isotherms at 77 K, using a fully automated model ASAP 2020 gas adsorption system (Micromeritics Instruments). Prior to the analysis, the samples were degassed for 2 h at 200 °C under a nitrogen atmosphere. The specific surface area (S_{BET}) was calculated using the BET method from the adsorption data over a relative pressure range of 0.05–0.30. The specific external surface area (S_{ext}) and the micropore volume ($V\mu$) were estimated by the t-plot method. The mesopore volumes (V_{mes}) are estimated by the Barrett–Joyner–Halenda (BJH) method [37].

The reducibility of the catalysts was investigated by temperature-programmed reduction (TPR), using a quadrupole mass spectrometer (Pfeiffer Vacuum Balzers, model QMS 200) equipped with a single Faraday detector, and controlled via a computer using the software Quadstar 422. Typically, 80 mg of sample were loaded in a U-shaped quartz microreactor and treated during 1 h with heat 500 °C, to remove water adsorbed on the sample surface. After cooling down to room temperature, the reduction gas (5 % H_2/Ar) was introduced at a flow rate of 60 STP

cm^3/min. The system was stabilized for 2 h, and then the temperature programmed to heat with a ramp of 10 °C/min up to 950 °C.

Catalytic activity

The catalytic activity of the natural material and the modified clays was evaluated in the reaction of CO oxidation. This reaction was carried out in a conventional continuous flow U-shaped quartz microreactor. The catalyst is placed over quartz wool and carborundum (Prolabo). A thermocouple in contact with the sample assures the right measure of temperature. The feed mixtures were prepared using mass flow controllers. The reaction products were analyzed by mass spectrometry, using a Pfeiffer Vacuum Balzers, model QMS 200 mass spectrometer with capabilities for quantitative analysis.

The light-off curves of CO oxidation (700, 10 °C/min) were obtained with a mixture (1 % CO, 20 % O_2 and 79 % He) at a total flow rate of 60 ml/min.

The catalysts were pre-activated in situ during 1 h at 500 °C with a mixture of 21 % O_2 in helium at a total flow rate of 60 ml/min and then stabilized at room temperature before the light-off curve started.

Results and discussion

XRD

Fig. 2 shows the XRD patterns of un-pillared, Al-pillared bentonite prepared by conventional and ultrasound methods and 2; 10 % manganese oxide impregnated catalysts. The XRD results shows a clear shift of the basal spacing (d_{001}) obtained for the PILC (17 and 18 Å for the samples prepared with and without ultrasound,

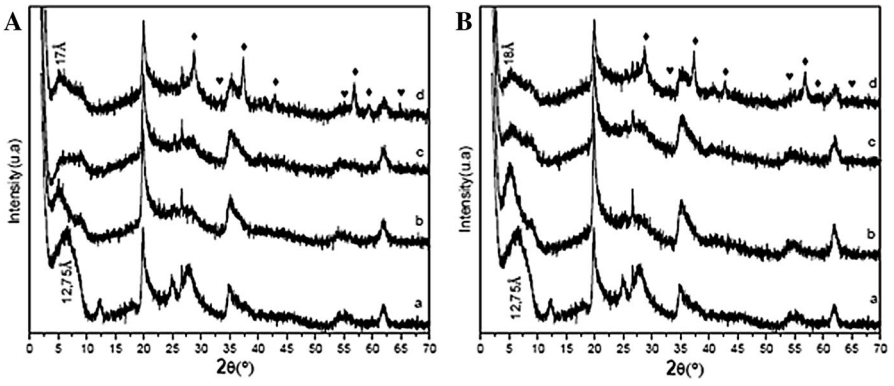

Fig. 2 X-ray diffraction patterns of bentonite, Al-pillared clay with and without ultrasound calcined at 500 °C and impregnated with two manganese loading 2 and 10 wt%. **a** (*a*) H; (*b*) (H–Al); (*c*) 2 % Mn (H–Al); (*d*) 10 % Mn (H–Al). **b** (*a*) H; (*b*) (H–Al)*; (*c*) 2 % Mn (H–Al)*; (*d*) 10 % Mn (H–Al)* The *symbols* correspond to MnO_2 (*closed diamond*) and Mn_2O_3 (*closed heart*)

respectively) with respect to the value obtained for the starting clay (12.75 Å), thus indicating that the clay was successfully pillared [22, 38–40].

The use of ultrasounds induces a slight increase in the basal spacing of the PILCs. As observed in Fig. 2, this sample shows a narrower and more defined signal characterized by a value of width at medium height clearly lower (FWHM = 0.5°, 2θ) than the one observed in the sample modified in the absence of ultrasounds (FWHM = 0.93°, 2θ).

The introduction of manganese does not modify the basal spacing of both pillared bentonite synthesised by the conventional and ultrasonic treatment. However, the line 001 becomes less intense and broader. These observations could indicate that impregnation produced a significant decrease in the ordering of the solids, but does not affect the layered structure of the supports.

Compared with Al-PILCs samples, no additional peaks characteristic of the manganese oxide phases were observed for PILCs modified with a 2 wt% of manganese. This may not require the absence of manganese oxides due to the fact that manganese is not present in sufficient quantities to be detected by XRD [33, 41]. However, in the XRD patterns of the catalysts impregnated with (10 wt% of Mn), new diffraction peaks appear. According to ASTM cards number 812261 and 780390, reflections at 28.68°, 37.2°, 42.82°, 56.65° and 59.37° correspond to manganese oxides in the form of MnO_2 while those at 32.9°, 55.1° and 65.1° reveal the presence of Mn_2O_3 [29, 30, 42]. Similar results were obtained by Kazin et al. [43] and Craciun [44] after calcinations in air of a Mn/SiO_2 catalyst at 500 °C.

Chemical analysis

The chemical compositions of all samples, as obtained from atomic absorption, are presented in Table 1. After pillaring via both conventional and ultrasonic treatment, an increase in the amounts of aluminum with a corresponding decrease in the amount of exchangeable cations highlights the success of Al incorporation in the solids. For the PILCs in the presence of ultrasound get similar results, with a little increase in the amount of Al compared with those obtained by conventional method. Meanwhile, this demonstrates the positive effect of ultrasound towards a greater introduction of the pillaring agent in the clay structure.

Table 1 Chemical analysis (wt%) of parent and modified interstratified illite–smectite, referred to ignited solids (0 % water)

Samples	SiO_2	Al_2O_3	Fe_2O_3	MgO	K_2O	Na_2O	CaO	MnO
H	60.76	23.8	8.25	2.36	1.54	2.37	0.86	–
(H–Al)	56.59	31.45	8.16	2.15	1.27	0.22	0.12	–
2 % Mn (H–Al)	55.19	31.48	7.69	2.09	1.21	0.18	0.13	1.9
10 % Mn (H–Al)	51.31	28.19	7.25	2	1.17	0.15	0.11	9.78
(H–Al)*	56.1	32.21	8.2	2	1.27	0.15	0.11	–
2 % Mn (H–Al)*	55.24	31.98	7.39	1.98	1.22	0.21	0.12	1.85
10 % Mn (H–Al)*	50.82	28.65	7.15	1.96	1.13	0.15	0.10	9.56

The impregnation of the manganese was also verified by chemical analysis. The increase in the MnO content in the Al-pillared bentonites after manganese impregnation shows that manganese was successfully inserted into the PILC structure. The incorporated amounts correspond to the employed amount, showing the effectiveness of the impregnation method [45].

Textural properties

The nitrogen adsorption/desorption isotherms of Al-PILC with and without ultrasound and the manganese oxide impregnated catalyst are shown in Fig. 3, and their textural parameters calculated from these isotherms are given in Table 2.

From the nitrogen the adsorption–desorption isotherms, it can be inferred that all our samples are micro and mesoporous materials. Indeed, nitrogen isotherms belong to a mixed type of International Union of Pure and Applied Chemistry (IUPAC) classification [46]. The initial part of the isotherms is of type I with uptake of nitrogen at very low relative pressure, which corresponds to adsorption in micropores. At intermediate and high relative pressures, the isotherms are of type IV with a narrow hysteresis loops of type H_3 associated with capillary condensation in mesopores of plate-like aggregates with open slit-shaped capillaries [47–50].

For the PILCs we observed an increase in the BET surface areas and in the porosity, mainly in microporosity, comparing with the purified clay. This increase confirms the successful pillaring of the bentonite.

It is important to emphasize that the use of ultrasound during the intercalation induces an improvement of textural properties compared to the conventional method. However, in the impregnated material, the specific surface area as well as the micropores volume decreased comparing to the Al-PILC prepared with both methods. This effect can be related to the partial blockage of the interlayer space of the clay by the impregnated metal oxides, which prevents the access of nitrogen [26, 48].

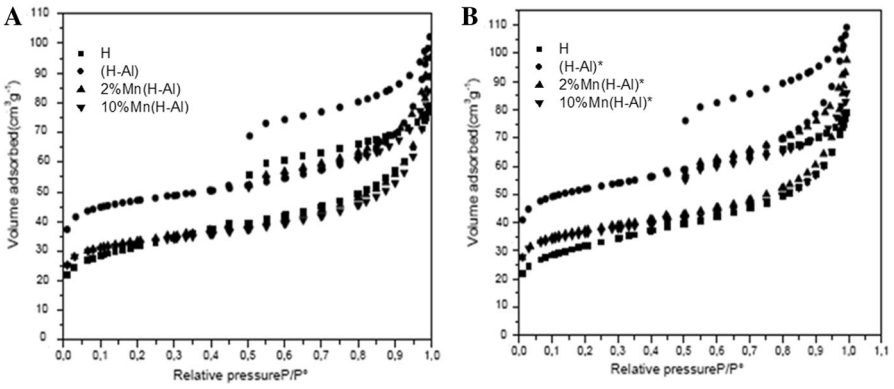

Fig. 3 Nitrogen adsorption/desorption isotherms of different samples. **a** Support prepared with conventional method and **b** support prepared with ultrasound method

Table 2 Textural properties of untreated, pillared and impregnated pillared samples

Samples	S_{BET} (m^2/g)	S_{ext} (m^2/g)	$S_{\mu p}$ (m^2/g)	Vp (cm^3/g)	$V_{\mu p}$ (cm^3/g)	V_{mes} (cm^3/g)
H	118	81	37	0.1504	0.019	0.1312
(H–Al)	165	56	109	0.2256	0.057	0.1686
2 % Mn (H–Al)	120	55	65	0.1883	0.033	0.1545
10 % Mn (H–Al)	116	46	70	0.1793	0.036	0.1426
(H–Al)*	174	63	111	0.2277	0.058	0.1695
2 % Mn (H–Al)*	133	62	71	0.1975	0.037	0.1599
10 % Mn (H–Al)*	128	52	76	0.1811	0.039	0.1412

Temperature-programmed reduction (TPR)

The catalysts were characterized by temperature programmed reduction in order to obtain information on the reducibility and oxidation state of the metals in the impregnated solids.

The H_2-TPR profiles of the starting clay, PILC with and without ultrasound (supports) and the impregnated clays with 2 and 10 wt% Mn are presented in Fig. 4. The unpillared interstratified illite–smectite reduction profile shows two reduction peaks at around 610 and 870 °C, with a shoulder at 400 °C. The peak at 610 °C can be assigned to the reduction of the magnetite to wustite ($Fe_3O_4 \rightarrow FeO$), and the high temperature peak (870 °C) may result from the reduction of wustite to metallic iron ($FeO \rightarrow Fe$). The shoulder at 400 °C has been previously associated to the reduction of the superficial iron oxides in the structure (hematite to magnetite; $Fe_2O_3 \rightarrow Fe_3O_4$) [40, 51]. The reduction profile of the pillared sample (H–Al) shows only one peak at 610 °C. This peak probably accounts for the total reduction of Fe species in this sample, much more accessible to reduction gas after pillaring.

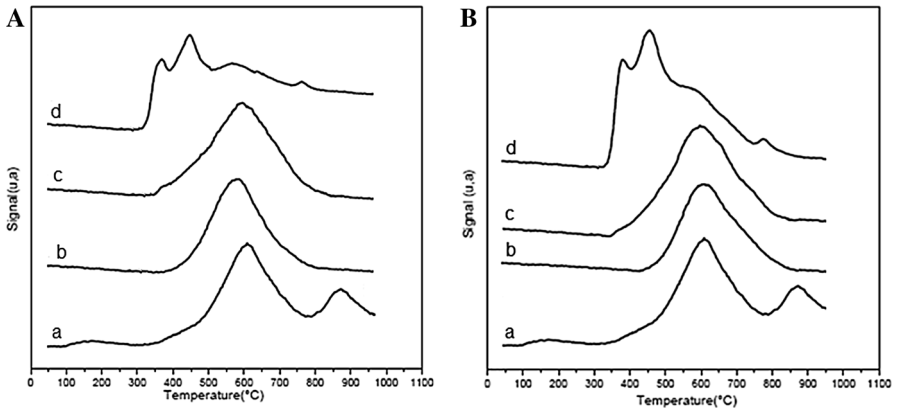

Fig. 4 Profiles H_2 reduction (H_2-TPR) of various samples **a** (support in absence of ultrasound): (*a*) H; (*b*) (H–Al); (*c*) 2 % Mn (H–Al); (*d*) 10 % Mn (H–Al). **b** (support in presence of ultrasound): (*a*) H; (*b*) (H–Al)*; (*c*) 2 % Mn (H–Al)*; (*d*) 10 % Mn (H–Al)*

The assignment of these peaks should be done with caution as they are well above the temperature used in the previous calcination of the samples. According to Fig. 4b, the use of ultrasound does not significantly affect the reduction behavior of this sample.

The incorporation of a 2 wt% of Mn leads to a broadening of the reduction peak at around 600 °C, which now accounts for the global reduction process of Fe and Mn species. In the case of the 10 % loaded sample, new maxima associated to MnO_x reduction are observed. According to the normal reduction scheme proposed for MnO_x [30, 42, 52], the peak at 380 °C involves the reduction of MnO_2 and Mn_2O_3 to Mn_3O_4, and the maxima at 455 °C could be assigned to the formation of MnO. Given that the peak which appears at 455 °C is significantly more intense than the one at 380 °C, we can conclude that the oxide Mn_2O_3 is a dominant form. As indicated for the manganese-free clays, it seems that the reducibility of the samples is not influenced by the use of ultrasounds.

Quantitative analyses on the H_2-TPR profiles can give the H_2 consumption of the samples, the total amount of hydrogen consumed of the reduction peaks estimated by integrating these profiles and the temperature of first peaks were compiled in Table 3.

In the case of the supports, a slight increase from 5.37 to 5.98 μ mol/g of hydrogen consumption in comparison to starting clay was verified, suggesting that when the clay is pillared, the newly formed porous structure promotes the reduction of iron oxides that are not initially accessible in the starting bentonite. It is important to emphasize that the increase of Mn content greatly enhances the hydrogen consumption. The catalyst obtained with 10 % Mn has the lowest reduction temperature and the highest hydrogen consumption, possibly providing a better catalytic system in the oxidation reaction.

Catalytic activity

The catalytic oxidation of CO by O_2 over unPILC and different synthesised catalysts was investigated at temperatures within the range of 25–700 °C. Figs. 5a and 5b show the light-off curves for the purified bentonite and manganese oxides with 2 and 10 wt% supported on Al-pillared bentonite synthesized by using both, the

Table 3 Quantitative results of H_2-TPR

Catalysts	Temperature[a] (°C)	H_2 consumption[b] (μmol/g)
H	610	5.37
(H–Al)*	600	5.98
2 % Mn (H–Al)*	590	6.02
10 % Mn (H–Al)*	380	10.41

[a] The temperature corresponding to the first reduction peak in Fig. 4b

[b] The total H_2 consumption of the reduction peaks calculated from room temperature to 950 °C

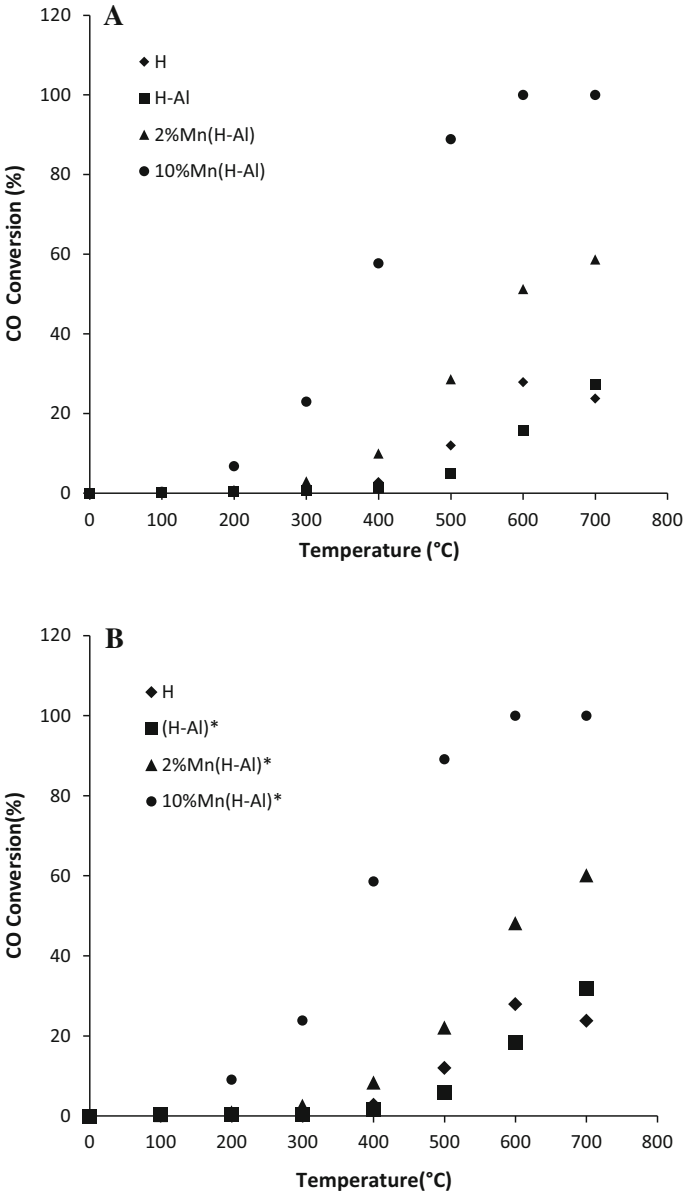

Fig. 5 CO conversion of parent clay, support prepared with (**b**) and without (**a**) ultrasound and impregnated catalysts, 1 % CO + 20 % O_2 in helium; catalyst weight = 0.25 g, total flow rate = 60 ml/min

conventional method and ultrasonic treatment. As it is shown in Fig. 5, the fresh and Al-PILCs presented the low catalytic activity for CO oxidation. Similar results were found by Carriazo et al. [25] and Pérez et al. [22] for bentonite clays from Colombia

Table 4 Maximum conversion and temperature at 50 % conversion

Samples	Temperature for 50 % conversion, T_{50} (°C)	Max. conversion (%)	Max. conversion temperature, T_{max} (°C)
H	–	30	600
(H–Al)	–	30	700
2 % Mn (H–Al)	600	60	700
10 % Mn (H–Al)	377	100	600
(H–Al)*	–	30	700
2 % Mn (H–Al)*	600	60	700
10 % Mn (H–Al)*	375	100	600

or Turkey [53]. In order to implement the structural and textural properties of Al-PILCs with activity for this reaction, they have been used as support for preparing MnO_x-supported catalysts. The results corresponding to the catalytic performance of two different manganese weight loadings (2 and 10 %) catalysts for the oxidation of CO are also included in Fig. 5 and Table 4. The influence of the addition of manganese is clearly deduced from these results. Indeed, the 2 % Mn sample shows a light-off temperature (T_{50}) of 600 °C, with a maximum conversion value of 60 % obtained at the higher temperature investigated (700 °C). Moreover, full CO conversion is obtained with the 10 % Mn catalyst, which also shows a significant decrease in the light-off temperature (375 °C) with respect to the lower loading sample 2 % Mn (T_{50} = 600 °C).

The activity of manganese oxides supported on bentonite based catalysts have been previously investigated for oxidation reactions such as the combustion of volatile organic compounds [54]. However, to the best of our knowledge, these are the first published results showing the activity of manganese oxides impregnated on bentonite PILCs for CO oxidation. In term of light-off temperature, our results are rather close to those reported by Zaki et al. [55] who obtained a CO conversion of 50 % at 340 °C using 10 % wt Mn_2O_3 supported on TiO_2 with Al_2O_3 and by Venkataswamy et al. [56] who obtained a light-off temperature of 374 °C for the manganese oxide supported on alumina (MnO_x/Al_2O_3).

Conclusion

As a summary of the results presented in this work, manganese oxide supported over inexpensive support PILCs were prepared and used as catalysts for oxidation of CO. XRD results show an increase of the basal spacing after pillaring and the conservation of the layered structure after Mn-impregnation. The results of N_2 adsorption reveal that the textural proprieties of PILC are enhanced. The TPR patterns showed a two-step reduction profile of manganese oxide and a three reduction peaks of iron. Activity tests in CO oxidation show that supported manganese oxide catalysts are found to be very suitable for this reaction. The higher loading catalysts (with 10 wt% of Mn) showed the highest catalytic activity for CO

oxidation compared to the lower loading samples (with 2 wt% of Mn), Al-PILC and starting clay, over which the CO conversion is up to 50 % at a temperature of 375 °C. It is important to mention that the use of ultrasound lead to an enhancement of the cristallinity and considerably reduces the pillaring duration, since in only 20 min treatment we observe similar catalytic performances with the catalysts prepared during 24 h by conventional method.

Acknowledgments The authors thank the project MINECO/FEDER/Ref: MAT2013-40823-R for financial support.

References

1. Royer S, Duprez D (2011) Catalytic oxidation of carbon monoxide over transition metal oxides. ChemCatChem 3:24–65
2. Gullotta F, Di Masi A, Ascenzi P (2012) Carbon monoxide: an unusual drug. IUBMB Life 64:378–386
3. Raub JA, Mathieu-Nolf M, Hampson NB, Thom SR (2000) Carbon monoxide poisoning—a public health perspective. Toxicology 145:1–14
4. Prockop LD, Chichkova RI (2007) Carbon monoxide intoxication: an updated review. J Neurol Sci 262:122–130
5. Raub JA, Benignus VA (2002) Carbon monoxide and the nervous system. Neurosci Biobehav Rev 26:925–940
6. Lawther PJ (1975) Carbon monoxide. Br Med Bull 31:256–260
7. Bateman DN (2012) Carbon monoxide. Medicine (Baltimore) 40:115–116
8. Biabani-Ravandi A, Rezaei M, Fattah Z (2013) Low-temperature CO oxidation over nanosized Fe–Co mixed oxide catalysts: effect of calcination temperature and operational conditions. Chem Eng Sci 94:237–244
9. Biabani-Ravandi A, Rezaei M (2012) Low temperature CO oxidation over Fe–Co mixed oxide nanocatalysts. Chem Eng J 184:141–146
10. Taylor SH, Rhodes C (2006) The oxidation of carbon monoxide at ambient temperature over mixed copper–silver oxide catalysts. Catal Today 114:357–361
11. Abdel Halim KS, Khedr MH, Nasr MI, El-Mansy AM (2007) Factors affecting CO oxidation over nanosized Fe_2O_3. Mater Res Bull 42:731–741
12. Gac W (2007) The influence of silver on the structural, redox and catalytic properties of the cryptomelane-type manganese oxides in the low-temperature CO oxidation reaction. Appl Catal B 75:107–117
13. Figueras F (1988) Pillared clays as catalysts. Catal Rev 30:457–499
14. Bergaya F, Aouad A, Mandalia T (2006) Chapter 7.5 pillared clays and clay minerals. Dev Clay Sci 1:393–421
15. Clearfield A (1996) Chapter 14—preparation of pillared clays and their catalytic properties. In: Moser WR (ed) Advances catalysis nanostructered material. Academic Press, San Diego, pp 345–394
16. Ding Z, Kloprogge JT, Frost RL (2001) Porous clays and pillared clays-based catalysts. Part 2: a review of the catalytic and molecular sieve applications. J Porous Mater 8:273–293
17. Gil A, Korili SA, Vicente MA (2008) Recent advances in the control and characterization of the porous structure of pillared clay catalysts. Catal Rev 50:153–221
18. Gil A, Gandía LM, Vicente MA (2000) Recent advances in the synthesis and catalytic applications of pillared clays. Catal Rev 42:145–212
19. Herling MM, Breu J (2014) The largely unknown class of microporous hybrid materials: clays pillared by molecules. Zeitschrift für Anorg und Allg Chemie 640:547–560
20. Kloprogge JT (1998) Synthesis of smectites and porous pillared clay catalysts: a review. J Porous Mater 5:5–41
21. Poncelet G, Fripiat JJ (2001) In: Smith J (ed) Handbook of Heterogeneous Catalysis, 2nd edn. Wiley, New York

22. Pérez A, Centeno MA, Odriozola JA, Molina R, Moreno S (2008) The effect of ultrasound in the synthesis of clays used as catalysts in oxidation reactions. Catal Today 133–135:526–529
23. Olaya A, Blanco G, Bernal S, Moreno S, Molina R (2009) Synthesis of pillared clays with Al–Fe and Al–Fe–Ce starting from concentrated suspensions of clay using microwaves or ultrasound, and their catalytic activity in the phenol oxidation reaction. Appl Catal B 93:56–65
24. Tomul F (2011) Effect of ultrasound on the structural and textural properties of copper-impregnated cerium-modified zirconium-pillared bentonite. Appl Surf Sci 258:1836–1848
25. Carriazo JG, Martínez LM, Odriozola JA, Moreno S, Molina R, Centento MA (2007) Gold supported on Fe, Ce, and Al pillared bentonites for CO oxidation reaction. Appl Catal B 72:157–165
26. Álvarez A, Moreno S, Molina R, Ivanova S, Centeno MA, Odriozola JA (2012) Gold supported on pillared clays for CO oxidation reaction: effect of the clay aggregate size. Appl Clay Sci 69:22–29
27. Martínez TLM, Domínguez MI, Sanabria N, Hernández WY, Moreno S, Molina R, Odriozola JA, Centeno MA (2009) Deposition of Al–Fe pillared bentonites and gold supported Al–Fe pillared bentonites on metallic monoliths for catalytic oxidation reactions. Appl Catal A 364:166–173
28. Xu Z, Inumaru K, Yamanaka S (2001) Catalytic properties of metal loaded silica-pillared manganese titanate for CO oxidation. Appl Catal A 210:217–224
29. Vicente MA, Belver C, Trujillano R, Rives V, Álvarez AC, Lambert JF, Korili SA, Gandia LM, Gil A (2004) Preparation and characterisation of Mn- and Co-supported catalysts derived from Al-pillared clays and Mn- and Co-complexes. Appl Catal A 267:47–58
30. Gandia LM, Vicente MA, Gil A (2000) Preparation and characterization of manganese oxide catalysts supported on alumina and zirconia-pillared clays. Appl Catal A 196:281–292
31. Li J, Li L, Wu F, Zhang L, Liu X (2013) Dispersion–precipitation synthesis of nanorod Mn_3O_4 with high reducibility and the catalytic complete oxidation of air pollutants. Catal Commun 31:52–56
32. Tian H, He J, Liu L, Wang D, Hao Z, Ma C (2012) Highly active manganese oxide catalysts for low-temperature oxidation of formaldehyde. Microporous Mesoporous Mater 151:397–402
33. Liu Y, Luo M, Wei Z, Xin Q, Ying P, Li C (2001) Catalytic oxidation of chlorobenzene on supported manganese oxide catalysts. Appl Catal B 29:61–67
34. Morales MR, Barbero BP, Cadús LE (2007) Combustion of volatile organic compounds on manganese iron or nickel mixed oxide catalysts. Appl Catal B 74:1–10
35. Pozan GS (2012) Effect of support on the catalytic activity of manganese oxide catalyts for toluene combustion. J Hazard Mater 221–222:124–130
36. Reynolds RC (1985) Newmod, a computer program for the calculation of one dimensional X ray diffraction patterns of mixed-layered clays. RC Reynolds 8:57–62
37. Deboer J (1964) Studies on pore systems in catalysts IV. The two causes of reversible hysteresis. J Catal 3:268–273
38. Katdare SP, Ramaswamy V, Ramaswamy AV (1999) Ultrasonication: a competitive method of intercalation for the preparation of alumina pillared montmorillonite catalyst. Catal Today 49:313–320
39. Katdare SP, Ramaswamy V, Ramaswamy AV (2000) Factors affecting the preparation of alumina pillared montmorillonite employing ultrasonics. Microporous Mesoporous Mater 37:329–336
40. Sanabria NR, Molina R, Moreno S (2009) Effect of ultrasound on the structural and textural properties of Al–Fe pillared clays in a concentrated medium. Catal Lett 130:664–671
41. Reed C, Lee YK, Oyama ST (2006) Structure and oxidation state of silica-supported manganese oxide catalysts and reactivity for acetone oxidation using ozone. J Phys Chem B 110:20–67
42. Zuo S, Huang Q, Li J, Zhou R (2009) Promoting effect of Ce added to metal oxide supported on Al pillared clays for deep benzene oxidation. Appl Catal B 91:204–209
43. Kazin PE, Tret YD (2008) Synthesis of magnetoresistive glass—ceramic composites in the SrO–MnO_x–SiO_2–La_2O_3 system. Catal Lett 2:34–36
44. Craciun R (1998) Structure/activity correlation for unpromoted and CeO_2-promoted. Catal Commun 55:25–31
45. Galeano LA, Gil A, Vicente MA (2011) Strategies for immobilization of manganese on expanded natural clays: catalytic activity in the CWPO of methyl orange. Appl Catal B 104:252–260
46. Sing KSW, Everett DH, Haul RAW, Moscou L, Pierotti RA, Rouquéol J, Siemieniewska T (1985) International union of pure commission on colloid and surface chemistry including catalysis * reporting physisorption data for gas/solid systems with special reference to the determination of surface area and porosity. Pure Appl Chem 57:603–619
47. Gregg SJ, Sing KS (1982) Adsorption, surface area and porosity. J Electrochem Soc 114(11):279C–279C

48. Lowell S, Shields JE, Thomas MA, Thommes M (2005) Characterization of porous solids and powders: surface area, pore size, and density. springer, Berlin
49. Schüth F, Sing KSW, Weitkamp J (2002) Handbook of porous solids. Wiley, Weinheim
50. Leofanti G, Padovan M, Tozzola G, Venturelli B (1998) Surface area and pore texture of catalysts. Catal Today 41:207–219. doi:10.1016/S0920-5861(98)00050-9
51. Jozwiak WK, Kaczmarek E, Maniecki TP et al (2007) Reduction behavior of iron oxides in hydrogen and carbon monoxide atmospheres. Appl Catal A 326:17–27
52. Li J, Li L, Cheng W, Wu F, Lu X, Li Z (2014) Controlled synthesis of diverse manganese oxide-based catalysts for complete oxidation of toluene and carbon monoxide. Chem Eng J 244:59–67
53. Tomul F, Balci S (2009) Characterization of Al, Cr-pillared clays and CO oxidation. Appl Clay Sci 43:13–20
54. Sambeth JE, Thomas HJ (2013) Volatile organic compound removal over bentonite-supported Pt, Mn and Pt/Mn monolithic catalysts. Reac Kinet Mech Cat 108:443–458
55. Zaki MI, Hasan MA, Pasupulety L, Fouad NE (1999) CO and CH total oxidation over manganese oxide supported on ZrO, TiO, TiO–AlO and SiO–AlO catalysts. New J Chem 23:1197–1202
56. Venkataswamy P, Jampaiah D, Lin F, Alxneit I, Reddy BM (2015) Applied surface science structural properties of alumina supported Ce–Mn solid solutions and their markedly enhanced catalytic activity for CO oxidation. Appl Surf Sci 349:299–309